

Electric-Field Dependence of the Effective Dielectric Constant in Graphene

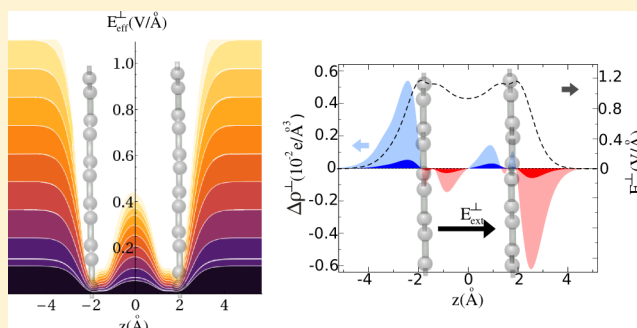
Elton J. G. Santos^{*,†} and Efthimios Kaxiras^{*,†,‡}

[†]School of Engineering and Applied Sciences, Harvard University, Cambridge, Massachusetts 02138, United States

[‡]Department of Physics, Harvard University, Cambridge, Massachusetts 02138, United States

ABSTRACT: The dielectric constant of a material is one of the fundamental features used to characterize its electrostatic properties such as capacitance, charge screening, and energy storage capability. Graphene is a material with unique behavior due to its gapless electronic structure and linear dispersion near the Fermi level, which can lead to a tunable band gap in bilayer and trilayer graphene, a superconducting-insulating transition in hybrid systems driven by electric fields, and gate-controlled surface plasmons. All of these results suggest a strong interplay between graphene properties and external electric fields. Here we address the issue of the effective dielectric constant (ϵ) in N -layer graphene subjected to out-of-plane (E_{ext}^{\perp}) and in-plane ($E_{\text{ext}}^{\parallel}$) external electric fields. The value of ϵ has attracted interest due to contradictory reports from theoretical and experimental studies. Through extensive first-principles electronic structure calculations, including van der Waals interactions, we show that both the out-of-plane (ϵ_{\perp}) and the in-plane (ϵ_{\parallel}) dielectric constants depend on the value of applied field. For example, ϵ_{\perp} and ϵ_{\parallel} are nearly constant (~ 3 and ~ 1.8 , respectively) at low fields ($E_{\text{ext}} < 0.01$ V/Å) but increase at higher fields to values that are dependent on the system size. The increase of the external field perpendicular to the graphene layers beyond a critical value can drive the system to an unstable state where the graphene layers are decoupled and can be easily separated. The observed dependence of ϵ_{\perp} and ϵ_{\parallel} on the external field is due to charge polarization driven by the bias. Our results point to a promising way of understanding and controlling the screening properties of few-layer graphene through external electric fields.

KEYWORDS: Graphene dielectric constant, multilayer graphene screening, tunable dielectric properties, electrostatic exfoliation, dielectric response



Electron–electron interactions play a central role in a wide range of electronic phenomena in graphene-based materials,^{1–9} from the reshaping of the Dirac cone^{10–12} in suspended graphene to observations of plasmaron quasiparticles¹³—bound states of charge carriers with plasmons—in doped layers. One of the main ingredients that determines the Coulomb interaction strength in those systems is screening, which can be characterized by graphene’s dielectric constant (ϵ). In fact, the large range of values for ϵ found by different experiments^{10–18} (from 2 to 15) has become a subject of considerable debate. The presence of substrates has likely played a role in the experimental attempts to measure the intrinsic dielectric constant in graphene as, for instance, was recently shown by angle-resolved photoemission spectroscopy (ARPES) experiments.¹² In practical terms the effective dielectric constant is defined by $\epsilon = (\epsilon_{\text{sub}} + \epsilon_{\text{vac}})/2$, with ϵ_{sub} and ϵ_{vac} the dielectric constant values for the substrate and vacuum, respectively. However, using this approach requires the detailed knowledge of the dielectric constant of the environment in which graphene is embedded, which is not always accessible. The determination of the intrinsic value of ϵ is therefore of great interest and importance. Here we find that

ϵ is electric-field dependent, with values in the range 3–16. We applied a spatially periodic sawtooth-like potential perpendicular (E_{ext}^{\perp}) or parallel ($E_{\text{ext}}^{\parallel}$) to the graphene layer which simulates the external field across the supercell. In the case of $E_{\text{ext}}^{\parallel}$, armchair nanoribbons of different width were utilized to create structures with periodic boundary conditions. The value of ϵ can be obtained by using $\epsilon_i = E_{\text{ext}}^i/E_{\text{net}}^i = 1 + 4\pi\chi^i$, with $i = \perp, \parallel$, where E_{net}^i is the net electric field in the slab or along the ribbon surface, and χ^i is the electric susceptibility (see details in Methods). The effective electric field either between the C -layers (E_{eff}^{\perp}) or along the ribbon width ($E_{\text{eff}}^{\parallel}$) is not constant, as discussed below.

Figure 1 displays how ϵ_{\perp} and ϵ_{\parallel} evolve with external fields. For out-of-plane polarization, ϵ_{\perp} is almost constant ~ 3.0 at low fields $E_{\text{ext}}^{\perp} < 0.001$ V/Å, independent of the number of layers. As E_{ext}^{\perp} is increased, ϵ_{\perp} takes larger values reaching $\epsilon_{\perp} = 13.2$ at $E_{\text{ext}}^{\perp} = 1.0$ V/Å for $N = 10$ layers. These values for ϵ_{\perp} agree very well with those found by many experimental groups.^{10–18} Notably,

Received: September 27, 2012

Revised: December 21, 2012

Published: January 22, 2013

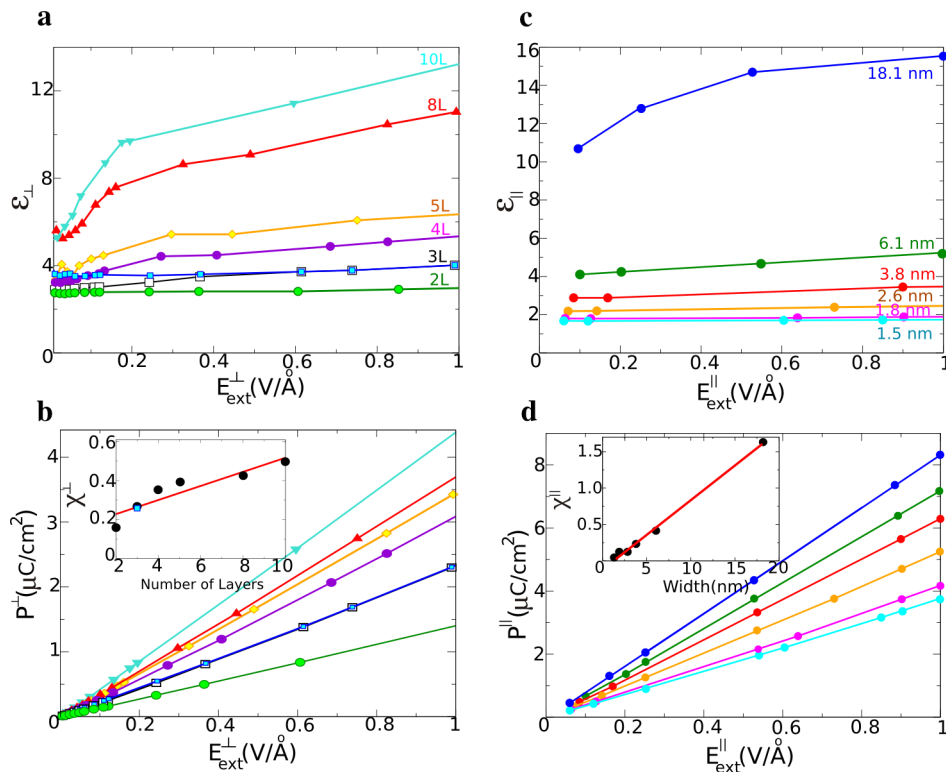


Figure 1. (a) Calculated ϵ_{\perp} as a function of E_{ext}^{\perp} (V/Å) for 2L–10L graphene. The AB stacking was used for all calculations, with the exception of 3L where ABC order (filled blue squares) was also considered. (b) P^{\perp} (μC/cm²) as a function of E_{ext}^{\perp} using the same labeling scheme for the graphene layers as in a. The inset shows the electric susceptibility χ^{\perp} versus the number of layers; the solid red curve corresponds to a linear fit. (c) ϵ_{\parallel} as a function of $E_{\text{ext}}^{\parallel}$ (V/Å) for armchair graphene nanoribbons of different width. (d) Polarization P^{\parallel} (μC/cm²) as a function of the external field $E_{\text{ext}}^{\parallel}$ for the ribbons calculated in c. The inset shows χ^{\parallel} as a function of the ribbon widths. The solid line corresponds to a linear fit.

monolayer (1L),^{10–14} bilayer (2L),^{15,16} and multilayer graphene or graphite^{17,18} give quite different response to an external electric field: the thicker the structure (more layers) the larger the value of ϵ_{\perp} , with a linear dependence of ϵ_{\perp} on the number of layers N at a fixed value of the field. The electric susceptibility χ^{\perp} extracted from the polarization P^{\perp} (Figure 1b) clearly shows this behavior. The in-plane dielectric constant ϵ_{\parallel} is nearly constant ~ 1.8 for small ribbon width (≤ 1.8 nm) in the whole range of external fields studied (see Figure 1c). With an increase of the width, ϵ_{\parallel} goes to higher values as a function of $E_{\text{ext}}^{\parallel}$, reaching $\epsilon_{\parallel} = 15.5$ at $E_{\text{ext}}^{\parallel} = 1.0$ V/Å for a width of 18.1 nm. This relation between ϵ_{\parallel} and the ribbon width is reflected in the linear behavior of the in-plane electric susceptibility χ^{\parallel} obtained from the polarization P^{\parallel} (Figure 1d). This suggests a similar dependence of χ^{\parallel} on the transverse ribbon direction as that observed for χ^{\perp} on the number of layers N . The polarizations P^{\perp} and P^{\parallel} are related by approximately a constant factor ~ 2 . This suggests that graphene behaves differently depending on the field polarization: it acts as a metal along the C-plane and as a semiconductor or semimetal perpendicular to it. This is in close agreement with spectroscopic ellipsometry measurements,¹⁸ performed with light polarized parallel and perpendicular to the carbon surface.

The origin of the electric-field-mediated tunable dielectric constant in graphene structures is shown schematically in Figure 2. We focus on the response of 2L graphene for out-of-plane field polarization as a simpler picture that can capture the essential features of this problem. The application of E_{ext}^{\perp} generates an interlayer charge-transfer which partially cancels the external field, producing the value of E_{eff}^{\perp} . At low E_{ext}^{\perp} all

values of E_{eff}^{\perp} are approximately constant (within the numerical accuracy of our model). At fields close to those used to modify the band gap of 2L graphene,^{1–3} 0.1 V/Å, E_{eff}^{\perp} is already dependent on position, with a maximum at the midpoint between the layers, and smaller values close to the C-atoms (Figure 2a). The induced charge densities, $\Delta\rho^{\perp}$, at different fields are shown in Figure 2b. The overall polarization charge is field-dependent and increases in magnitude with the external field intensity as discussed above. The integration of $\Delta\rho^{\perp}$ along the direction perpendicular to the layers (z coordinate), using the Poisson equation $\nabla^2 V(z)^{\perp} = -\Delta\rho^{\perp}/\epsilon_0$, where ϵ_0 is the vacuum permittivity, results in a response electric field E_{ρ}^{\perp} (dashed line in Figure 2b) which screens the external electric field, that is, $E_{\text{eff}}^{\perp} \approx E_{\text{ext}}^{\perp} - E_{\rho}^{\perp}$. Similar features are observed for the in-plane polarization. Figure 2c shows $E_{\text{eff}}^{\parallel}$ as function of the position for different values of $E_{\text{ext}}^{\parallel}$. The external field decays as it penetrates along the ribbon which indicates that an effective field $E_{\text{eff}}^{\parallel}$ is created, with a charge accumulation at the positive potential edge and a corresponding depletion at the negative one (Figure 2d). This charge-polarization generates a response field (E_{ρ}^{\parallel}) along the ribbon width that screens the external field (dashed line in Figure 2d) in a similar manner as that observed for out-of-plane polarization.

We address next the dependence of ϵ_{\perp} and ϵ_{\parallel} on the number of graphene layers N and on the ribbon width. In Figure 3 we plot E_{eff}^{\perp} and $E_{\text{eff}}^{\parallel}$ as a function of the position z for $N = 3, 5, 7$ (3a) and different ribbon widths: 3.8, 6.1, 18.1 nm (3b). For out-of-plane polarization, the application of E_{ext}^{\perp} on thicker graphene structures generates higher E_{eff}^{\perp} in the first few layers. For instance, in the $N = 10$ case, the maximum value of E_{eff}^{\perp}

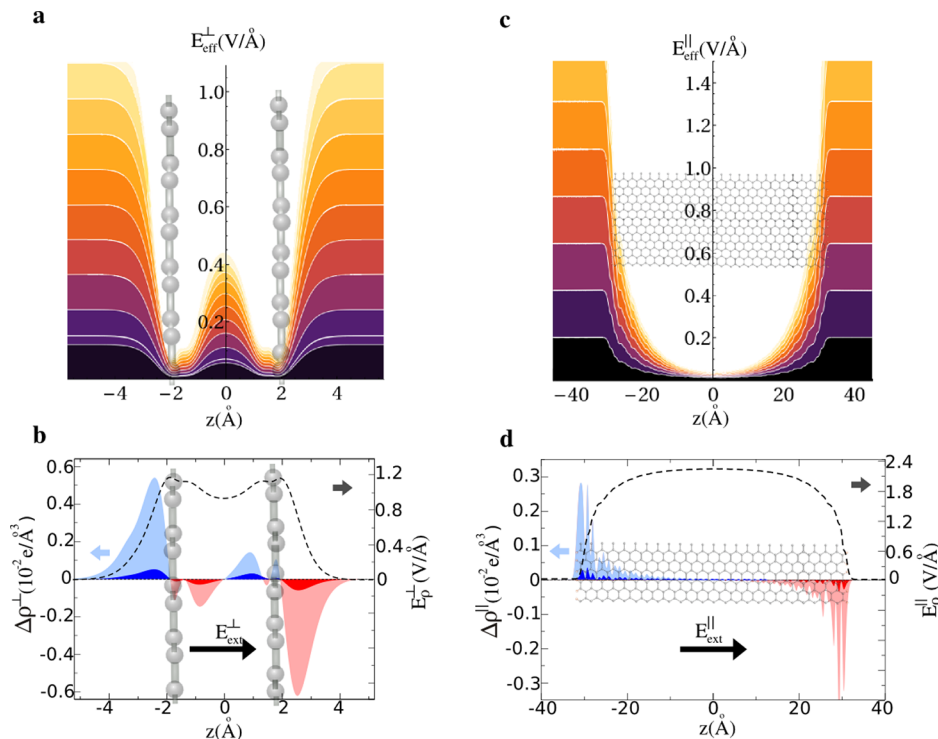


Figure 2. (a) E_{eff}^{\perp} as a function of the interlayer distance at different external fields E_{ext}^{\perp} for bilayer graphene. The plate geometry is shown on the background picture. (b) Induced charge densities, $\Delta\rho^{\perp} = \rho(E_{\text{ext}}^{\perp}) - \rho(0)$, in $e/\text{\AA}^3$, between the two C-planes. The bolder and lighter shaded curves correspond to $E_{\text{ext}}^{\perp} = 0.12 \text{ V}/\text{\AA}$ and $E_{\text{ext}}^{\perp} = 1.22 \text{ V}/\text{\AA}$, respectively. The dashed line curve corresponds to the electric field generated by the induced charge (E_p^{\perp}) at $E_{\text{ext}}^{\perp} = 1.22 \text{ V}/\text{\AA}$. The large black arrow shows the direction of E_{ext}^{\perp} relative to the bilayer structure. (c) $E_{\text{eff}}^{\parallel}$ as a function of the distance along the ribbon width. The ribbon is 6.1 nm wide with armchair edges saturated by H atoms. (d) $\Delta\rho^{\parallel}$ along the ribbon surface for $E_{\text{ext}}^{\parallel} = 0.20 \text{ V}/\text{\AA}$ and $E_{\text{ext}}^{\parallel} = 2.24 \text{ V}/\text{\AA}$, with the same legend as in b. The dashed line curve corresponds to E_p^{\parallel} generated by the in-plane polarization charge at $E_{\text{ext}}^{\parallel} = 2.24 \text{ V}/\text{\AA}$.

between the two graphene layers at $z = 4z_0$ and $3z_0$ is 3.2 times larger than that between the layers at $z = 3z_0$ and $2z_0$. In deeper layers, the field decays further reaching even smaller values. As ϵ_{\perp} is determined by the value of E_{eff}^{\perp} throughout the slab, the enhancement in the value of the dielectric constant with the number of layers N is directly related to the reduction of field in the innermost regions of the structure which leads to a lower average value. The nonlinear nature of the screening in multilayer graphene is the main reason for this behavior.^{19–21} In the case of in-plane polarization, similar arguments can be used based on the ribbon width being the main variable instead of the thickness in the multilayer structure.

There is a limit on the magnitude of E_{ext}^{\perp} that can be applied to the system. Figure 4 shows the total energy for bilayer graphene as a function of the interlayer distance. The calculated equilibrium distance (z_0) is 3.4 \AA . For $E_{\text{ext}}^{\perp} = 0.0 \text{ V}/\text{\AA}$, a van der Waals barrier (E_{vdW}) of $E_{\text{vdW}} = 28.1 \text{ meV}/\text{\AA}$ prevents the separation of the two layers from z_0 to infinity. For $E_{\text{ext}}^{\perp} > 0$ the value of E_{vdW} diminishes, indicating that the C-planes become less bound. At $E_{\text{ext}}^{\perp} = 1.8 \text{ V}/\text{\AA}$, the two planes of 2L graphene can be easily separated with $E_{\text{vdW}} = 3.3 \text{ meV}/\text{\AA}$. The existence of a field that can be used to exfoliate graphene was previously observed by experiments to prepattern few-layer graphene onto substrates in integrated circuits.²² Therefore, E_{ext}^{\perp} should be carefully applied to just tune the electronic and screening features, without leading to exfoliation.

To summarize, we have used first-principles electronic structure calculations to demonstrate that the effective dielectric constant in multilayer or single-layer graphene is tunable by an external electric field. The effect we describe may

partially explain experimentally observed results that to date had been attributed to unknown interface structure. This electric-field mediated tuning of the dielectric properties provides an additional degree of freedom in the design and modification of graphene-based materials, opening new possibilities for efficient control of electronic device properties.

Methods. The simulations reported here are based on density-functional-theory calculations using the SIESTA code.²³ We have used the nonlocal van der Waals density functional for the exchange-correlation term.²⁴ We used a double- ζ polarized basis and norm-conserving Troullier-Martins pseudopotentials.²⁵ Atomic coordinates were allowed to relax using a conjugate-gradient algorithm until all forces were smaller in magnitude than 0.01 eV/ \AA . Relevant lattice constants (in-plane and out-of-plane) were optimized for each system. To avoid interactions between layer images the distance between periodic images of the graphene structures along the direction perpendicular or parallel to the C-atom plane was set at 20 \AA . The resolution of the real-space grid used to calculate the Hartree and exchange-correlation contribution to the total energy was chosen to be equivalent to 150 Ry plane-wave cutoff. The number of k -points was chosen according to the Monkhorst–Pack²⁶ scheme and was set to the equivalent of a $44 \times 44 \times 1$ grid in the two-atom primitive unit cell of graphene, which gives well converged values for all the calculated properties. We used a Fermi–Dirac distribution with an electronic temperature of $k_B T = 21 \text{ meV}$.

The values of the induced electric fields along each direction were calculated taking a derivative with respect to the distance of the averaged electrostatic potential ($\langle V_H(\mathbf{r}) \rangle$) by finite

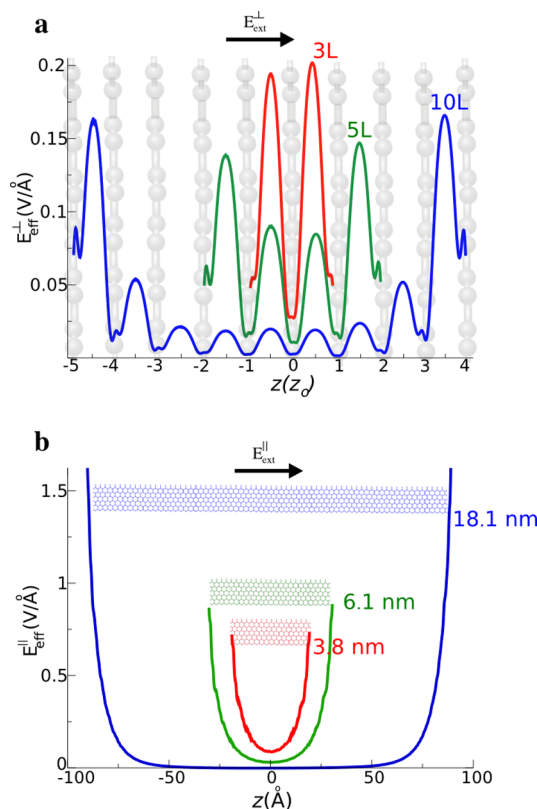


Figure 3. (a) E_{eff}^{\perp} as a function of the interlayer position ($z_0 = 3.41$ Å) for 3L (red curve), 5L (green curve), and 10L (blue) graphene (the graphene layers are shown in the background). The black arrow on top shows the orientation of E_{ext}^{\perp} . (b) $E_{\text{eff}}^{\parallel}$ as a function of the position along the ribbon width. Three different widths are shown: 3.8 nm, 6.1 nm, and 18.1 nm. The direction of $E_{\text{ext}}^{\parallel}$ is marked by the black arrow. The applied external field in both cases is 0.50 V/Å.

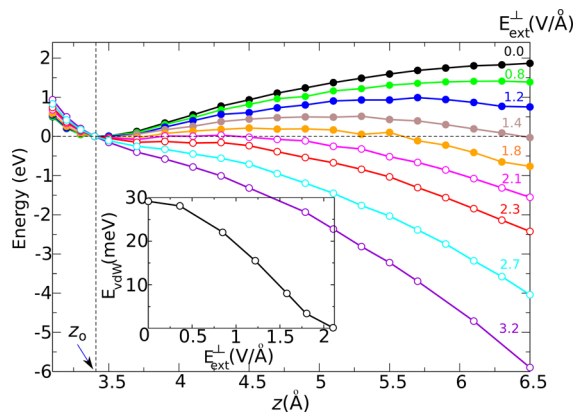


Figure 4. Energy per cell versus interlayer distance for different values of E_{ext}^{\perp} in V/Å. The vertical dashed line indicates the equilibrium position z_0 . The inset shows the dependence of E_{vdW} on E_{ext}^{\perp} .

differences between a calculation at zero and a finite value of the external field. $\langle V_H(\mathbf{r}) \rangle$ was calculated taking the planar average over planes parallel to the C surface, followed by its convolution with a filter function to eliminate oscillations and conserve only those features that are relevant on a macroscopic scale.²⁷ This defines the electric displacement D or the external electric field E_{ext}^i ($i = \perp, \parallel$) outside the slabs after the self-consistency. The net electric field E_{net}^i is calculated using the equation $E_{\text{net}}^i = E_{\text{inp}}^i / (1 + 4\pi\chi^i(1 - d/c))$, where E_{inp}^i is the input

field in the calculation before the self-consistency, d is the thickness of the graphene structure, and c is the total length of the supercell in the direction of the external field. χ^i is calculated using $\chi^i = (1/4\pi)(E_{\text{inp}}^i - E_{\text{ext}}^i)/(-E_{\text{inp}}^i + E_{\text{ext}}^i + (1 - d/c))$. This procedure accounts for the creation of compensating dipole moment induced by the application of the external field.^{28,29} $\Delta\rho^{\perp,\parallel}$ were calculated using a similar procedure, taking the total charge density distribution (ionic plus electronic) as the initial quantity. The polarizations $P^{\perp,\parallel}$ were calculated by the integration of $\Delta\rho^{\perp,\parallel}$ through $\nabla \cdot \mathbf{P}(\mathbf{r}) = -\Delta\rho(\mathbf{r})$ for each field polarization. We use the same procedure as shown in ref 29.

AUTHOR INFORMATION

Corresponding Author

*E-mail: esantos@seas.harvard.edu; kaxiras@physics.harvard.edu.

Notes

The authors declare no competing financial interest.

ACKNOWLEDGMENTS

We thank Tomas Palacios and Philip Kim for helpful discussions and Daniel Sanchez-Portal, Javier Junquera, and David Goldhaber-Gordon for comments on the manuscript. We have used the Extreme Science and Engineering Discovery Environment (XSEDE), supported by NSF grant numbers TG-DMR120073, TG-DMR120049, and TG-PHY120021.

REFERENCES

- (1) Mak, K. F.; Lui, C. H.; Shan, J.; Heinz, T. F. Observation of an Electric-Field-Induced Band Gap in Bilayer Graphene by Infrared Spectroscopy. *Phys. Rev. Lett.* **2009**, *102*, 256405–256409.
- (2) Zhang, Y.; Tang, T. T.; Girit, C.; Hao, Z.; Martin, M. C.; Zettl, A.; Crommie, M. F.; Shen, Y. R.; Wang, F. Direct observation of a widely tunable bandgap in bilayer graphene. *Nature* **2009**, *459*, 820–823.
- (3) Castro, E. V.; Novoselov, K. S.; Morozov, S. V.; Peres, N. M. R.; dos Santos, J. M. B. L.; Nilsson, J.; Guinea, F.; Geim, A. K.; Castro-Neto, A. H. Biased Bilayer Graphene: Semiconductor with a Gap Tunable by the Electric Field Effect. *Phys. Rev. Lett.* **2007**, *99*, 216802–216806.
- (4) Lui, C. H. L.; Zhiqiang Mak, K. F.; Cappelluti, E.; Heinz, T. F. Observation of an electrically tunable band gap in trilayer graphene. *Nat. Phys.* **2011**, *7*, 944–947.
- (5) Bao, W.; Jing, L.; Velasco, J.; Lee, Y.; Liu, G.; Tran, D.; Standley, B.; Aykol, M.; Cronin, S. B.; Smirnov, D.; Koshino, M.; McCann, E.; Bockrath, M.; Lau, C. N. Stacking-dependent band gap and quantum transport in trilayer graphene. *Nat. Phys.* **2011**, *7*, 948–952.
- (6) Zhang, L.; Zhang, Y.; Camacho, J.; Khodas, M.; Zaliznyak, I. The experimental observation of quantum Hall effect of $\ell=3$ chiral quasiparticles in trilayer graphene. *Nat. Phys.* **2011**, *7*, 953–957.
- (7) Allain, A.; Han, Z.; Bouchiat, V. Electrical control of the superconducting-to-insulating transition in graphene as metal hybrids. *Nat. Mater.* **2012**, *11*, S90–S94.
- (8) Fei, Z.; Rodin, A. S.; Andreev, G. O.; Bao, W.; McLeod, A. S.; Wagner, M.; Zhang, L. M.; Zhao, Z.; Thieme, M.; Dominguez, G.; Fogler, M. M.; Neto, A. H. C.; Lau, C. N.; Keilmann, F.; Basov, D. N. Gate-tuning of graphene plasmons revealed by infrared nano-imaging. *Nature* **2012**, *487*, 82–85.
- (9) Chen, J.; Badioli, M.; Alonso-Gonzalez, P.; Thongrattanasiri, S.; Huth, F.; Osmond, J.; Spasenovic, M.; Centeno, A.; Pesquera, A.; Godignon, P.; Zurutuza-Elorza, A.; Camara, N.; de Abajo, F. J. G.; Hillenbrand, R.; Koppens, F. H. L. Optical nano-imaging of gate-tunable graphene plasmons. *Nature* **2012**, *487*, 77–81.
- (10) Elias, D. C.; Gorbachev, R. V.; Mayorov, A. S.; Morozov, S. V.; Zhukov, A. A.; Blake, P.; Ponomarenko, L. A.; Grigorieva, I. V.;

Novoselov, K. S.; Guinea, F.; Geim, A. K. Dirac cones reshaped by interaction effects in suspended graphene. *Nat. Phys.* **2011**, *7*, 701–704.

(11) Siegel, D. A.; Park, C. H.; Hwang, C.; Deslippe, J.; Fedorov, A. V.; Louie, S. G.; Lanzara, A. Many-body interactions in quasi-freestanding graphene. *Proc. Natl. Acad. Sci.* **2011**, *108*, 11365–11370.

(12) Hwang, C.; Siegel, D. A.; Mo, S. K.; Regan, W.; Ismach, A.; Zhang, Y.; Zettl, A.; Lanzara, A. Fermi velocity engineering in graphene by substrate modification. *Sci. Rep.* **2012**, *2*, 590.

(13) Bostwick, A.; Speck, F.; Seyller, T.; Horn, K.; Polini, M.; Asgari, R.; MacDonald, A. H.; Rotenberg, E. Observation of Plasmarons in Quasi-Freestanding Doped Graphene. *Science* **2010**, *328*, 999–1002.

(14) Wang, Y.; Brar, V. W.; Shytov, A. V.; Wu, Q.; Regan, W.; Tsai, H. Z.; Zettl, A.; Levitov, L. S.; Crommie, M. F. Mapping Dirac Quasiparticles near a Single Coulomb Impurity on Graphene. *Nat. Phys.* **2012**, *8*, 653–657.

(15) Sanchez-Yamagishi, J. D.; Taychatanapat, T.; Watanabe, K.; Taniguchi, T.; Yacoby, A.; Jarillo-Herrero, P. Quantum Hall Effect, Screening, and Layer-Polarized Insulating States in Twisted Bilayer Graphene. *Phys. Rev. Lett.* **2012**, *108*, 076601–076606.

(16) Fallahazad, B.; Hao, Y.; Lee, K.; Kim, S.; Ruoff, R. S.; Tutuc, E. Quantum Hall effect in Bernal stacked and twisted bilayer graphene grown on Cu by chemical vapor deposition. *Phys. Rev. B* **2012**, *85*, 201408–201413.

(17) Reed, J. P.; Uchoa, B.; Joe, Y. I.; Gan, Y.; Casa, D.; Fradkin, E.; Abbamonte, P. The Effective Fine-Structure Constant of Freestanding Graphene Measured in Graphite. *Science* **2010**, *330*, 805–808.

(18) Jellison, G. E.; Hunn, J. D.; Lee, H. N. Measurement of optical functions of highly oriented pyrolytic graphite in the visible. *Phys. Rev. B* **2007**, *76*, 085125–085133.

(19) Castro Neto, A. H.; Guinea, F.; Peres, N. M. R.; Novoselov, K. S.; Geim, A. K. The electronic properties of graphene. *Rev. Mod. Phys.* **2009**, *81*, 109–162.

(20) Jang, C.; Adam, S.; Chen, J.-H.; Williams, E. D.; Das Sarma, S.; Fuhrer, M. S. Tuning the Effective Fine Structure Constant in Graphene: Opposing Effects of Dielectric Screening on Short- and Long-Range Potential Scattering. *Phys. Rev. Lett.* **2008**, *101*, 146805–146809.

(21) Kuroda, M. A.; Tersoff, J.; Martyna, G. J. Nonlinear Screening in Multilayer Graphene Systems. *Phys. Rev. Lett.* **2011**, *106*, 116804–116808.

(22) Liang, X.; Chang, A. S. P.; Zhang, Y.; Harteneck, B. D.; Choo, H.; Olynick, D. L.; Cabrini, S. Electrostatic Force Assisted Exfoliation of Prepatterned Few-Layer Graphenes into Device Sites. *Nano Lett.* **2009**, *9*, 467–472.

(23) Soler, J. M.; Artacho, E.; Gale, J. D.; Garcia, A.; Junquera, J.; Ordejon, P.; Sánchez-Portal, D. The SIESTA method for ab initio order-*N* materials simulation. *J. Phys.: Condens. Matter* **2002**, *14*, 2745–2779.

(24) Dion, M.; Rydberg, H.; Schröder, E.; Langreth, D. C.; Lundqvist, B. I. Van der Waals Density Functional for General Geometries. *Phys. Rev. Lett.* **2004**, *92*, 246401–246405.

(25) Troullier, N.; Martins, J. L. Efficient pseudopotentials for plane-wave calculations. *Phys. Rev. B* **1991**, *43*, 1993–2006.

(26) Monkhorst, H. J.; Pack, J. D. Special points for Brillouin-zone integrations. *Phys. Rev. B* **1976**, *13*, 5188–5192.

(27) Junquera, J.; Cohen, M. H.; Rabe, K. M. Nanoscale smoothing and the analysis of interfacial charge and dipolar densities. *J. Phys.: Condens. Matter* **2007**, *19*, 213203–213237.

(28) Junquera, J. Private communication, 2013.

(29) Meyer, B.; Vanderbilt, D. Ab initio study of BaTiO₃ and PbTiO₃ surfaces in external electric fields. *Phys. Rev. B* **2001**, *63*, 205426–205436.